JOURNAL OF SOLID STATE CHEMISTRY 72, 376–389 (1988)

Long-Period Stacking Variants in the Homologous Series $U_2La_{2n-2}O_{2n}S_{n+1}$

T. OKABE,* G. VAN TENDELOO, J. VAN LANDUYT, S. AMELINCKX,† AND M. GUITTARD‡

RUCA (Universiteit Antwerpen), Groenenborgerlaan 171, B 2020 Antwerpen, Belgium

Received March 24, 1987

Compounds with composition $(UOS)_2(La_2O_2S)_{n-1}$ form a homologous series, with structures derived from the hexagonal structure of La_2O_2S by the introduction of periodic nonconservative planar interfaces along which the excess of sulfur is accommodated. The structures on either side of the interfaces are related by a rotation over π about the normal to the interfaces. Pseudo-incommensurate diffraction patterns result from compounds containing lamellae with different thicknesses corresponding to fractional n values. The conclusions are based on high-resolution images, the interpretation of which is supported by image simulation. © 1988 Academic Press, Inc.

1. Introduction

Interface modulated ordered structures can be formed in a variety of ways. The periodic interfaces may separate domain slabs, the structures of which are related by *translations,* which are usually lattice vectors but not superlattice vectors. This is the case for periodic anti- or out-of-phase boundaries, forming long-period alloy structures, for periodic crystallographic shear planes leading to shear structures, for periodic stacking faults giving rise to polytypic structures, and for discommensuration walls forming often incommensurate structures.

The periodic interfaces may also separate slabs related by a *rotation* symmetry operation which is not a symmetry operation of the basic structure. Well-known examples are periodic inversion boundaries in noncentrosymmetric structures, for which successive domain slabs are related by an inversion operation (*1*). The periodic interfaces may also separate domain slabs related by a mirror operation (*2*), by a glide-mirror operation (*3*), or by a rotation over π (*4*).

Some long-period superstructures may contain periodic lamellae of two different crystal structures and chemical compositions, which are juxtaposed in an epitaxial relationship along the interfaces. Such materials are called mixed-layer compounds. They form a broad class of long-period superstructures to which the above-mentioned superstructures also belong as far as their diffraction behavior is concerned. In

* Permanent address: Department of Physics, Toyama University, Toyama 930, Japan.

† Also at SCK/CEN, B 2400 Mol, Belgium.

‡ Université R. Descartes, 4 rue de l'Observatoire F 75270, Paris, France.

0022-4596/88 $3.00

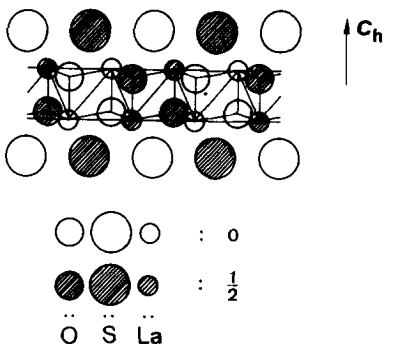

FIG. 1. Schematic representation of the hexagonal structure of La_2O_2S, as viewed along the close-packed direction of the sulfur sublattice.

Ref. (*5*) we have given a description of the characteristic features of the diffraction patterns resulting from such structures.

In the present paper we discuss a homologous series of quaternary compounds in the system U–La–O–S, the superstructures of which vary in a systematic manner with the composition. The structures contain periodic arrangements of two types of slabs which are related by translations as well as by rotations; the interfaces are nonconservative and their presence allows accommodation of the excess of one of the chemical species.

The materials were prepared by heating the appropriate mixture of La_2O_2S and UOS at a temperature of 1400°C in an atmosphere of argon for 2 h. It is also possible to use a mixture of La_2S_3 and $2La_2O_3$ instead of 3 La_2O_2S, the remaining treatment being the same. The UOS is obtained by reaction of H_2S with U_3O_8 at 1050°C in an amorphous carbon crucible.

2. Structural Considerations

The compounds under discussion can be considered as members of a pseudobinary system of two ternaries, $(UOS)_2(La_2O_2S)_{n-1} \equiv U_2La_{2n-2}O_{2n}S_{n+1}$. Their crystal structures can be derived from that of La_2O_2S by the periodic introduction of nonconservative planar interfaces (*6*). The structures are also closely related to those of the cerium oxysulfides, $Ce_4O_4S_3$ (*7*) and $Ce_6O_6S_4$ (*8*), which contain a mixture of tri- and tetravalent cerium. The sites of tetravalent cerium can be occupied by uranium, and correspond then to the $n = 2$ and $n = 3$ members of the series.

The hexagonal structure of La_2O_2S (*9*) is represented schematically in Fig. 1 as viewed along the close-packed directions. It consists of $(La_2O_2)_n$ bilayers perpendicular to the c axis. Each oxygen atom in the bilayers is surrounded by a tetrahedron of lanthanum atoms as indicated in Fig. 1. Two successive bilayers are separated by close-packed layers of sulfur atoms.

The addition of UOS results in the substitution of La by U; moreover, there is now an excess of sulfur atoms. Substitution of one group of La_2O_2S by $U_2O_2S_2$, i.e., substitution of two lanthanum atoms by two uranium atoms, results in an excess of one sulfur atom. Substitution in compound n of two lanthanum atoms by two uranium atoms results in an excess of sulfur of 1 part in n. For $n = 2$, for instance, the sulfur content has to be increased by 50% as compared with pure La_2O_2S. It is found that the basic structure remains essentially the same, the sulfur atoms being incorporated into planar interfaces.

The simplest way to visualize the results of this substitution is to note that the contents of the orthorhombic cell represented in Fig. 2a remain the same, although the slabs of these cells are rearranged. If the slabs are assumed to represent the sublattice of sulfur atoms, this arrangement can be shown schematically as in Figs. 2b, c, and d for three different compounds $n = 2$, $n = 3$, and $n = \frac{5}{2}$.

The planar interfaces are parallel to the $(010)_o$ planes (subindex o refers to orthorhombic). In the lattice planes coinciding with such a planar interface the sul-

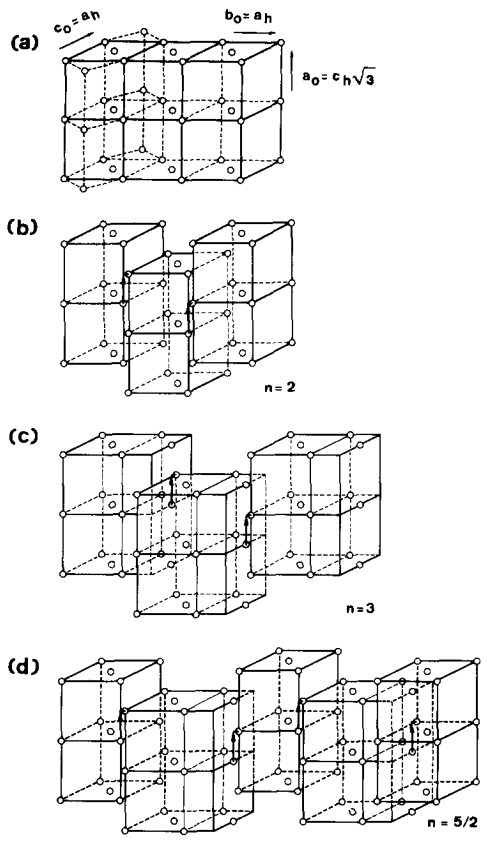

FIG. 2. Spatial representation of several members of the homologous series of compounds $U_2La_{2n-2}O_{2n}S_{n+1}$. Only the sulfur sublattice is represented. (a) Basic structure which can be compared with Fig. 1. (b) 2 $\bar{2}$ structure ($n = 2$). (c) 3 $\bar{3}$ structure ($n = 3$). (d) 2 $\bar{3}$ structure ($n = \frac{5}{2}$).

fur concentration is twice that in the other (010) lattice planes of the sulfur sublattice. According to the above considerations, one in n (010) lattice planes of the sulfur sublattice must become a nonconservative interface to accommodate the excess sulfur.

The structure determination described in Ref. (*6*) revealed that these interfaces are in fact not simple crystallographic shear planes. The shear vector acting on the sulfur sublattice is $\frac{1}{2}[100]$. Moreover, the structures in successive slabs are related by a rotation over π about an axis parallel with the direction $[010]_0$. This rotation is not evident from Fig. 2, because only the sulfur atoms are represented.

Finally, the sulfur arrangement in the interfaces is no longer planar but slightly wavy with the troughs being parallel with the $[001]_0$ direction; this causes a small increase in the lattice parameter b_0 of the long-period structures as compared with b_0 of the basic structure, each interface contributing an extra dilatation of about 0.09 nm (*6*). Thus, the exact shear vector has in fact a small component ε along the b direction.

We can represent the stacking variants with symbols such as 2 $\bar{2}$, 3 $\bar{3}$, 4 $\bar{4}$; the numbers indicate the numbers of "units" in a slab, where a "unit" contains one sulfur layer, i.e., as outlined by the heavy line in Fig. 3a.

We shall show that more complicated sequences such as 2 $\bar{3}$, 3 $\bar{4}$, 4 $\bar{5}$ and 4 $\bar{4}$ 3 $\bar{4}$ 4 $\bar{3}$ also occur. An example corresponding to $n = \frac{5}{2}$ is represented in Fig. 2d.

The relative displacements of successive

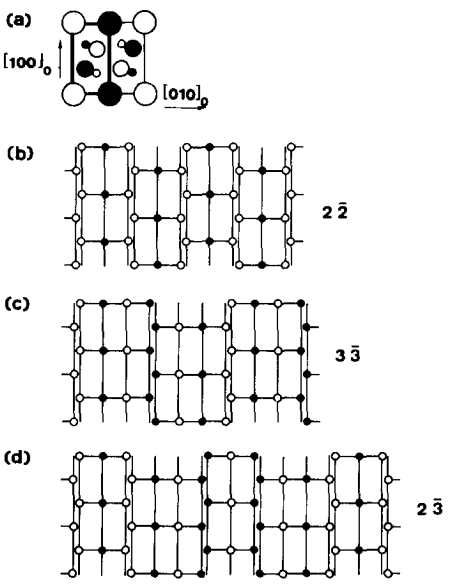

FIG. 3. Schematic representation, viewed along a close-packed direction of the sulfur lattice of several compounds of the series. (a) Basic structure. (b) 2 $\bar{2}$ structure. (c) 3 $\bar{3}$ structure. (d) 2 $\bar{3}$ structure.

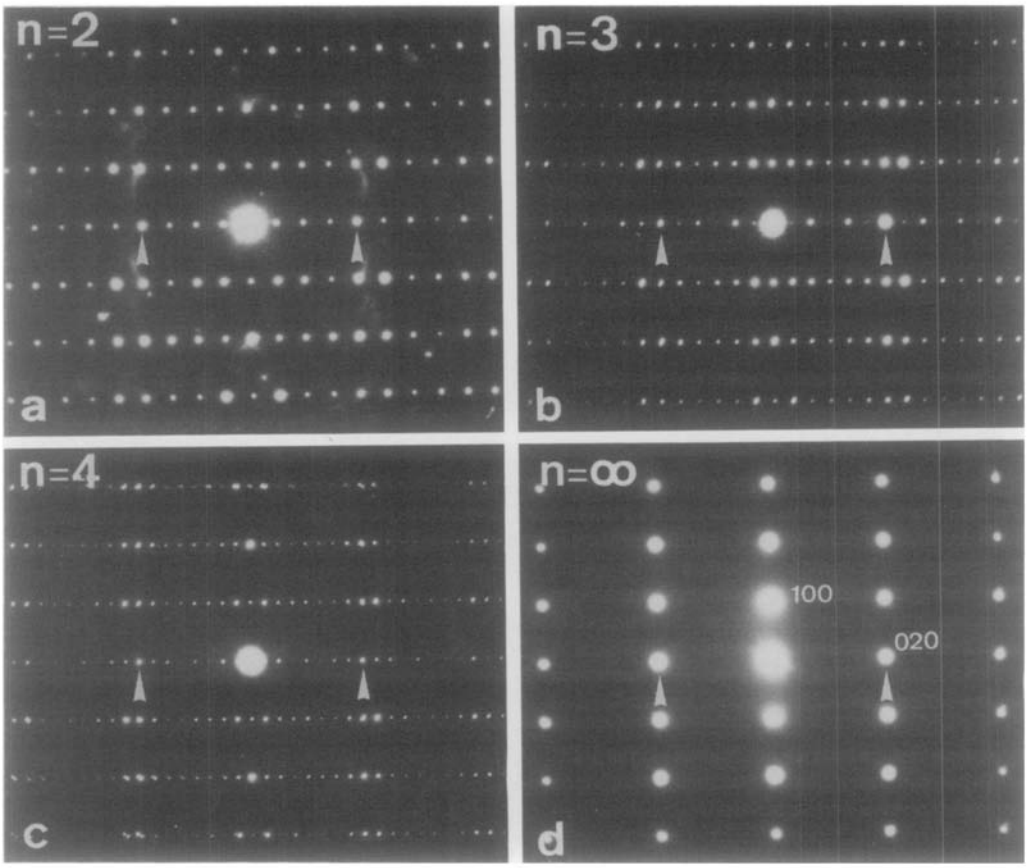

FIG. 4. Diffraction patterns of the compounds with n = integer taken along the zone [001]. (a) $n = 2$. (b) $n = 3$. (c) $n = 4$. (d) $n = \infty$.

slabs are $[\frac{1}{2}\varepsilon 0]$ in all cases, as represented schematically in Figs. 2b–d.

3. Electron Diffraction Patterns

3.1. Geometry of the Patterns

The electron diffraction patterns of compounds $n = 2$, $n = 3$, $n = 4$, and $n = \infty$ are shown in Fig. 4 all at the same magnification and camera constant. All the patterns can be indexed on an orthorhombic lattice with the following parameters:

$a = 0.693$ nm	$a = 0.6953$ nm
$b = 1.471$ nm	$b = 2.171$ nm
$(n = 2)$	$(n = 3)$
$c = 0.4024$ nm	$c = 0.4053$ nm

They correspond with some of the different stacking variants also revealed in the X-ray study (*6*). The number n is in fact given by half the number N of intervals between two successive spots due to the basic structure, which are usually the most intense ones. To locate the basic spots we use Fig. 4d, which is the reference diffraction pattern of the basic structure. We then note that the basic spots in the diffraction pattern of the stacking variants are slightly displaced in the b direction with respect to those in the reference pattern in a sense corresponding to a somewhat larger interplanar spacing. The deviation is largest for the compounds with the smallest n values; this is due to the in-

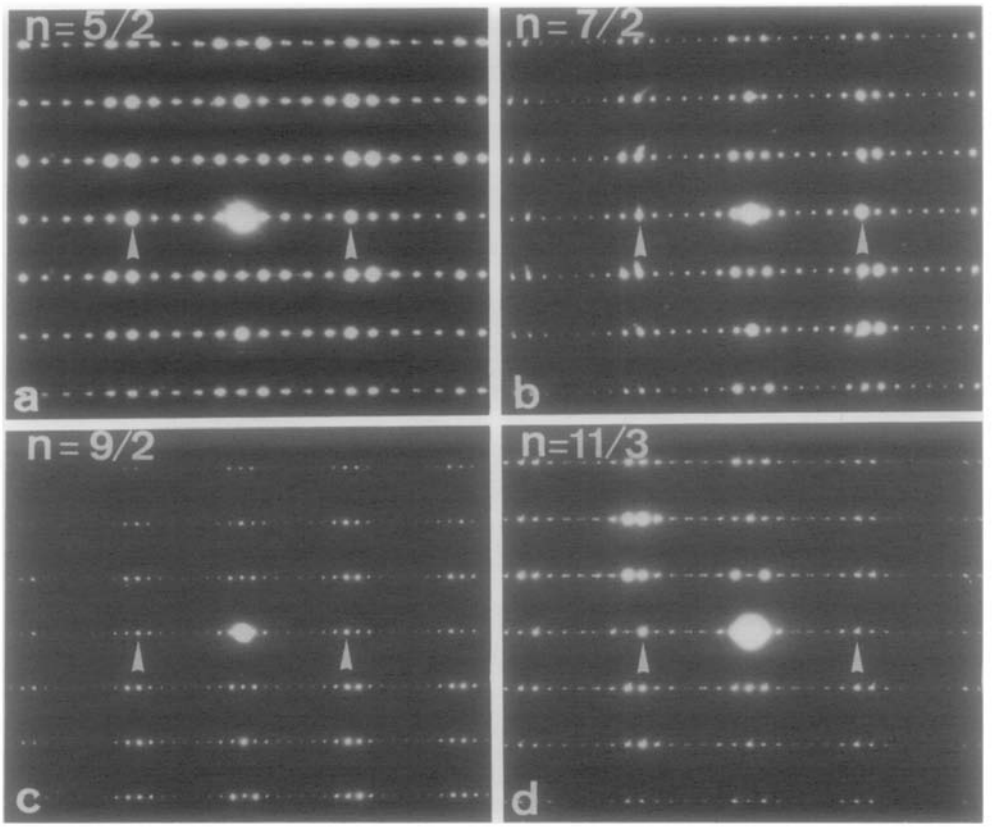

FIG. 5. Diffraction patterns of the compounds with n = fraction. (a) $n = \frac{5}{2}$. (b) $n = \frac{7}{2}$. (c) $n = \frac{9}{2}$. (d) $n = \frac{11}{3}$.

creased "width" of the double sulfur layer along the interfaces, which is relatively more important in the compounds with small n, and which increases somewhat the b parameter (see Appendix).

We have also observed electron diffraction patterns such as those in Figs. 5 and 6a which correspond to nonintegral values of n.

In Fig. 5a the distance between fundamental spots is divided into five intervals: $N = 5$ and thus $n = 2\frac{1}{2}$. In Fig. 5b $N = 7$ and $n = 3\frac{1}{2}$. In Fig. 5c this distance is divided into $N = 9$ intervals corresponding to $n = 4\frac{1}{2}$. Finally, in Fig. 5d the diffraction pattern is pseudo-incommensurate, i.e., the satellite sequences belonging to different basic reflections do not match where they meet; the number of intervals is $N = 7\frac{1}{3}$., i.e., $n = \frac{11}{3}$. We shall see that high-resolution electron microscopy suggests a straightforward interpretation of such fractional n values. This last observation clearly shows that the weak spots must be interpreted as satellites of the basic spots.

3.2. *Intensity Considerations*

The spot intensities vary in a periodic manner along the b^* rows, the maxima occurring at spot positions due to the basic structure. This behavior is characteristic of mixed layer compounds (5).

The spots along b^* of compounds corresponding with an *integral* number n (Fig.

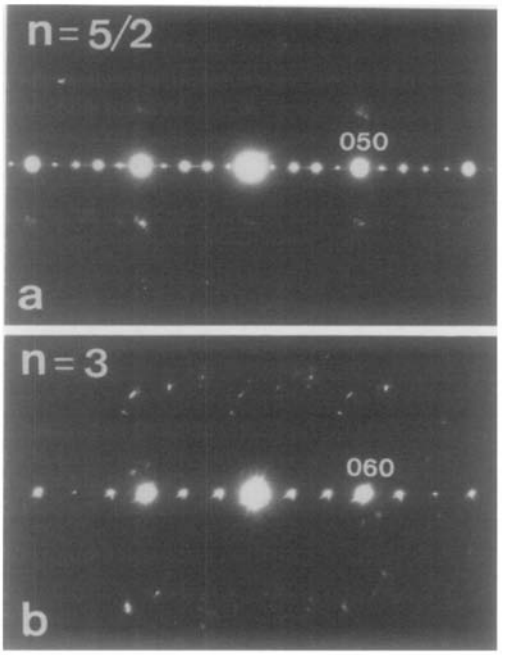

FIG. 6. Central rows of the diffraction patterns of two compounds under conditions where double diffraction is minimized. (a) $n = \frac{5}{2}$. (b) $n = 3$. Note the absence of the odd-order satellites in (b) and their relative weakness in (a).

4), are alternatively strong and weak, i.e., the spots with k = even are systematically stronger than those with k = odd, which are "quasi-extinct." The quasi-extinction is least pronounced for compound $n = 2$, but is quite pronounced for $n = 3$ and $n = 4$. The "extinctions" are of course destroyed in part by double diffraction effects, which are most pronounced in the vicinity of strong spots.

Tilt experiments were carried out for compounds $n = \frac{5}{2}$ (Fig. 6a) and $n = 3$ (Fig. 6b). In the diffraction pattern of compound $n = \frac{5}{2}$ the satellite spots in the row $0k0$ remain of comparable intensity whatever the tilt angle; i.e., no real extinctions can be found even after elimination of most of the double diffraction (Fig. 6a). Nevertheless, we note that the two central spots are systematically more intense than the others. One thus finds again that the even-order satellites are more intense than the odd-order ones. Furthermore, the superstructure spots must be considered as satellites. On the other hand, in compound $n = 3$ the satellites of odd order, i.e., with k = odd, can be made very weak by eliminating as far as possible the contribution from double diffraction (Fig. 6b).

It is further worth noting that there is a trend for the superstructure spots with h = odd, k = odd as well as those with h = even, k = even, i.e., $h + k$ = even, to be more intense than the others. This is especially visible for spots in the vicinity of row $h00$; it suggests a quasi-centering of the superstructure as projected along the c direction. This trend is again slightly more pronounced for compounds $n = 2$, 3, and 4 (Figs. 4a–c) than for those with fractional n values (Figs. 5a–c).

These qualitative features of the electron diffraction pattern are in good agreement with the models. The "extinctions" in the $0k0$ row of reflections are due to the fact that along the b direction the same crystal slabs occur, displaced over $b/2 + \varepsilon$ and rotated over π about this axis; this is equivalent to the presence in the superstructure of a twofold screw axis along the b axis. The fact that the slabs are furthermore displaced over $\frac{1}{2}[100]$ does not affect the $0k0$ reflections. The twofold screw axis leads to extinctions only if the two crystal slabs are of equal thickness, this is not the case for $n = 5$ which has the structure symbol $2\bar{3}$, but it is true for $n = 6$: $(3\bar{3})$.

The reason why even for $n = 2$ the "extinctions" are not complete is that the periodic presence of double sulfur layers introduces a period that causes $0k0$ Bragg reflections at the k = odd positions. This is not the case for $n = 3$. These double sulfur layers have a smaller influence at higher n values.

The relative weakness of the reflections for which $h + k$ = odd suggests that the

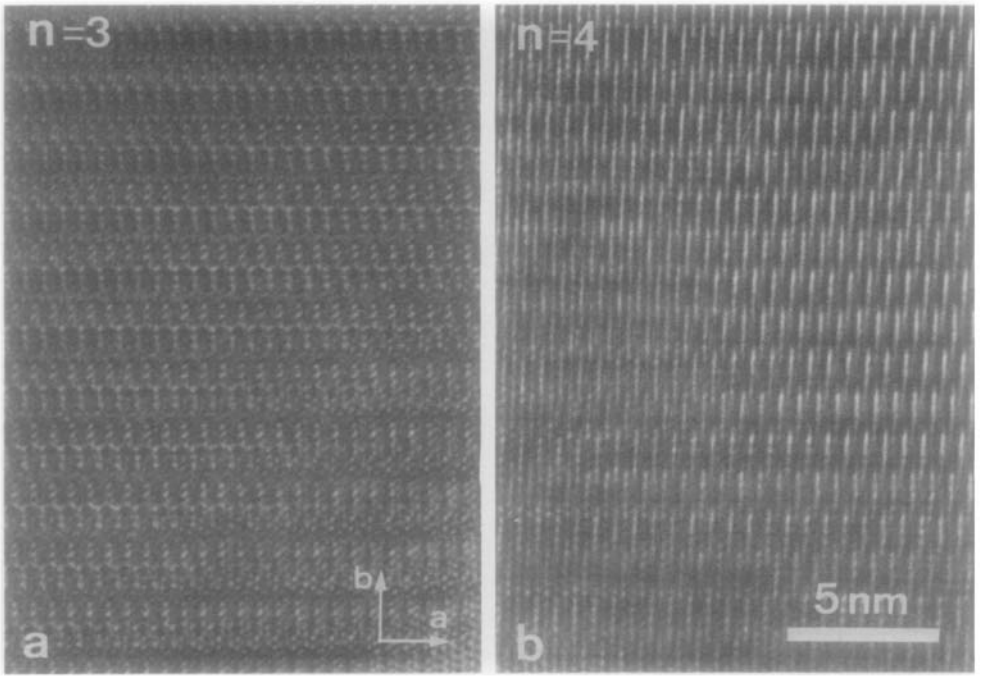

FIG. 7. High-resolution electron microscope images along the [001] zone of the compounds with n = integer. (a) $n = 3$. (b) $n = 4$.

projected structure along the c zone should be centered to a good approximation. If we ignore the fact that successive slabs are rotated over π, this is indeed the case in the compounds with n = integer. The "centering" is best approximated for reflections in the vicinity of the $h00$ row (Fig. 4c), because for such reflections the two slabs look the same since the succession and spacing of ($h00$) layers is the same in both.

4. High-Resolution Images

High-resolution images were obtained along the [001] zone because along this direction the lattice parameter is the shortest (~0.4 nm) and because the atoms occur in chemically homogeneous columns. Reflections corresponding to spacings down to 0.14 nm were included in the objective aperture. The images are in general rather complicated, but for certain defocus values and thicknesses an imaging code is obtained that has a simple relationship with the crystal structure. The two simplest examples are reproduced in Figs. 7a and b, which correspond respectively to the diffraction patterns in Figs. 4b and c. The first refers to compound $n = 3$ (structure symbol $3\ \bar{3}$) and the second to compound $n = 4$ (structure symbol $4\ \bar{4}$). The most striking feature is the occurrence of short equidistant bright segments or bars in successive strips parallel to the a axis. In successive strips along the b axis the segments are interleaved. The distance between these bars is the same in all images (Figs. 7 and 8) taken under the same conditions.

Sometimes the bright bars are resolved in three or four bright spots in compounds n = 3 and $n = 4$, respectively; this is shown clearly in Figs. 7a and b. The images correspond to structures $3\ \bar{3}$ and $4\ \bar{4}$. The same type of contrast also occurs in the images in

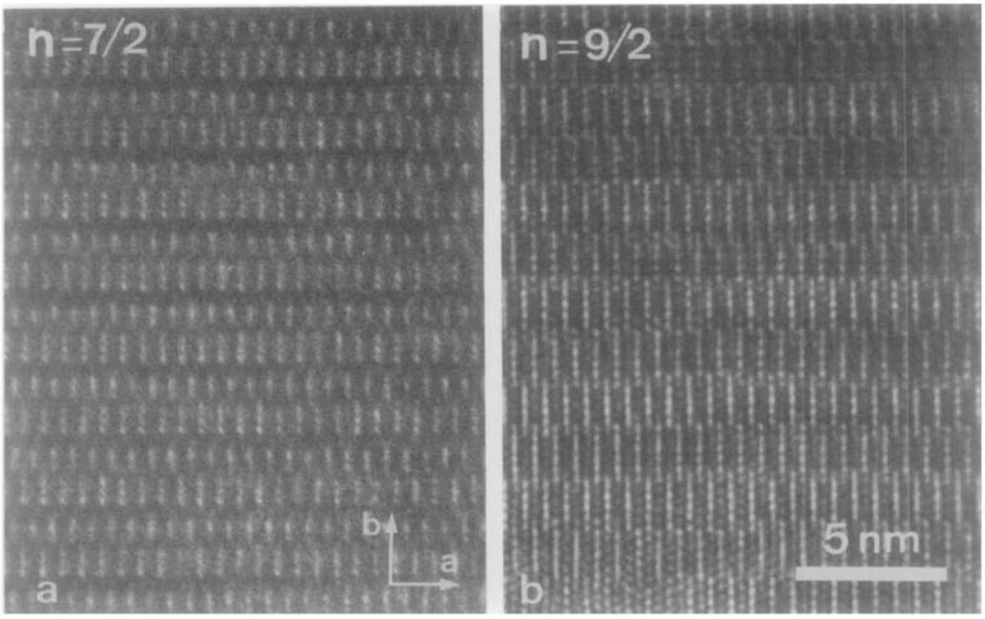

FIG. 8. High-resolution electron microscope images along the [001] zone of the compounds with n = fraction. (a) $n = \frac{7}{2}$. (b) $n = \frac{9}{2}$.

Figs. 8a and b, which correspond to the diffraction patterns in Figs. 5b and c, respectively. In these cases it is evident that the short bright bars alternate in length in successive strips. In Fig. 8a the lengths of the bars are in the ratio 4:3 in successive strips. In Fig. 8b the ratio of the lengths of the bright bars in successive strips is 4:5. Also, the numbers of bright dots have the same ratios; i.e., there are 4 dots in one strip and 5 in the next.

It is clear that the images in Figs. 7 and 8 suggest that slabs with a constant period along the a direction, but with two different lengths along the b direction, alternate. In Fig. 8a, these alternating slabs contain 3 and 4 units, whereas in Fig. 8b slabs containing 4 and 5 units alternate regularly. The structure symbols are thus $3\,\bar{4}$ and $4\,\bar{5}$, respectively.

These images explain why the n values deduced from the diffraction patterns (Figs. 5b and c) are 3.5 and 4.5, respectively, leading to $N = 7$ and $N = 9$ intervals between basic spots. The models for such structures are represented schematically in Figs. 3d and 2d.

More complicated sequences may occur as can be deduced from Fig. 9a, which is imaged in a mode not very different from that used for Figs. 7 and 8. Instead of short bright bars, short arrays of closely spaced bright dots occur regularly. From the magnified part (Fig. 9b) it is clear that the separation of bright dot arrays is still the same as that of the bars. Successive strips have widths now of 4, 4, and 3 units, which is consistent with the fractional value of $n = \frac{11}{3}$ deduced from the diffraction pattern (Fig. 5d). The structure symbol is now $4\,\bar{4}\,3\,\bar{4}\,4\,\bar{3}$.

Finally, the first and simplest representative of the series, i.e., $n = 2$, is imaged in Fig. 10. The imaging code is quite different from that obtained for the other compounds, and a simple relationship with the structural model is not evident and can only be deduced by means of image simulations.

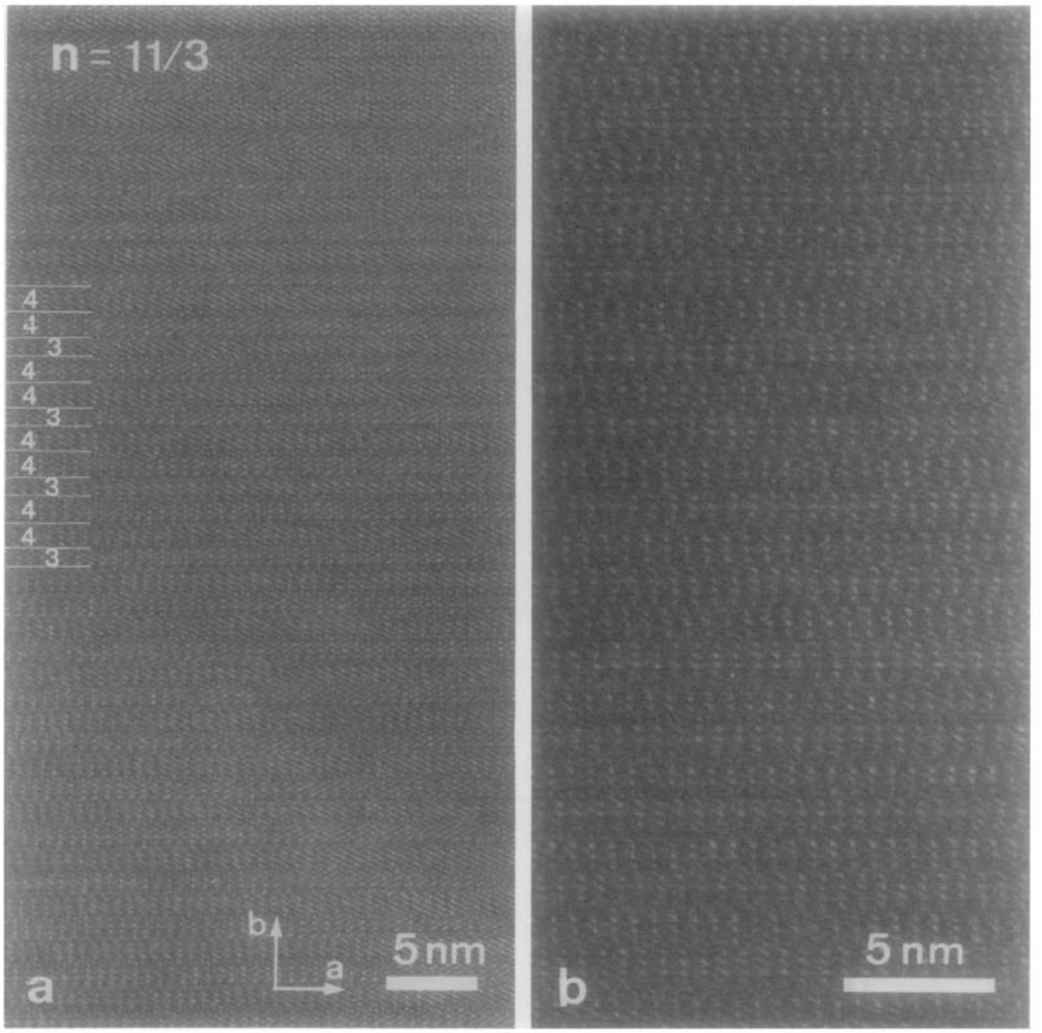

FIG. 9. High-resolution electron microscope images along the [001] zone of compound $n = \frac{11}{3}$ which gives rise to a pseudo-incommensurate diffraction pattern; the stacking sequence is $4\,\bar{4}\,3\,\bar{4}\,4\,3\ldots$. (a) Low magnification. (b) High magnification.

We have also imaged one of the ternary compounds on which the structure determination of the quaternary compounds is based. Images of the $Ce_4O_4S_3$ ($n = 2$) compound are reproduced in Fig. 11. Since for this compound the atomic coordinates have been determined (*8*), we shall be able to compare the observed image with computed images (see next section).

5. Image Simulations

In the absence of knowledge of the exact atomic positions for the quaternary compounds we have simulated the [001] zone images of the isomorphous ternary compound $Ce_4O_4S_3$ and $Ce_6O_6S_4$ based on the atomic coordinates given in Ref. (*9*). Use was made of the direct space method devel-

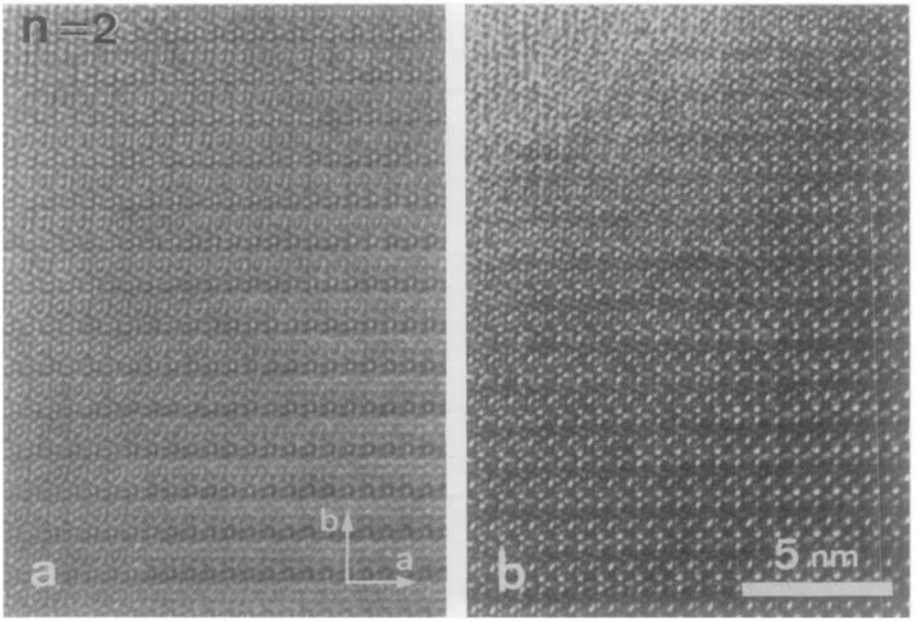

FIG. 10. High-resolution electron microscope image of compound $n = 2$. The imaging code is quite different from that for Figs. 7 and 8.

oped by Coene and Van Dyck (*10*). The instrumental parameters were: accelerating voltage, 200 kV; spherical aberration constant, $C_s = 1.2$ mm; focus spread Δf, 7 nm; and beam divergence, 8×10^{-4} rad.

A matrix of images was computed for two compounds, $n = 2$ and $n = 3$, for thicknesses in the range 4.5–20 nm and for defocus values from +30 to −150 nm. As the general features were very similar in the two cases, we have reproduced here only the relevant part of the matrix for $Ce_4O_4S_3$ ($n = 2$). The images are very sensitive to the imaging conditions, as can be seen in Fig. 12, but it is possible to fit certain areas of the experimental images with the com-

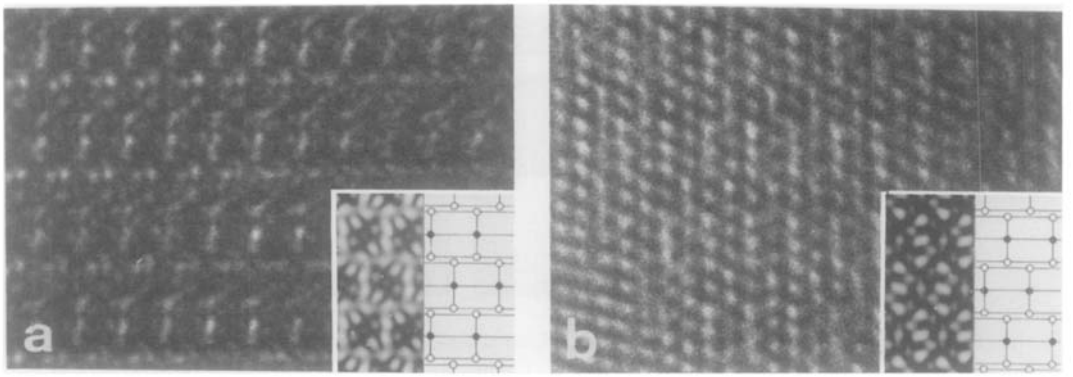

FIG. 11. High-resolution images of the ternary compound $Ce_4O_4S_3$ ($n = 2$). Comparison of model, experimental image, and simulated image at the same magnification.

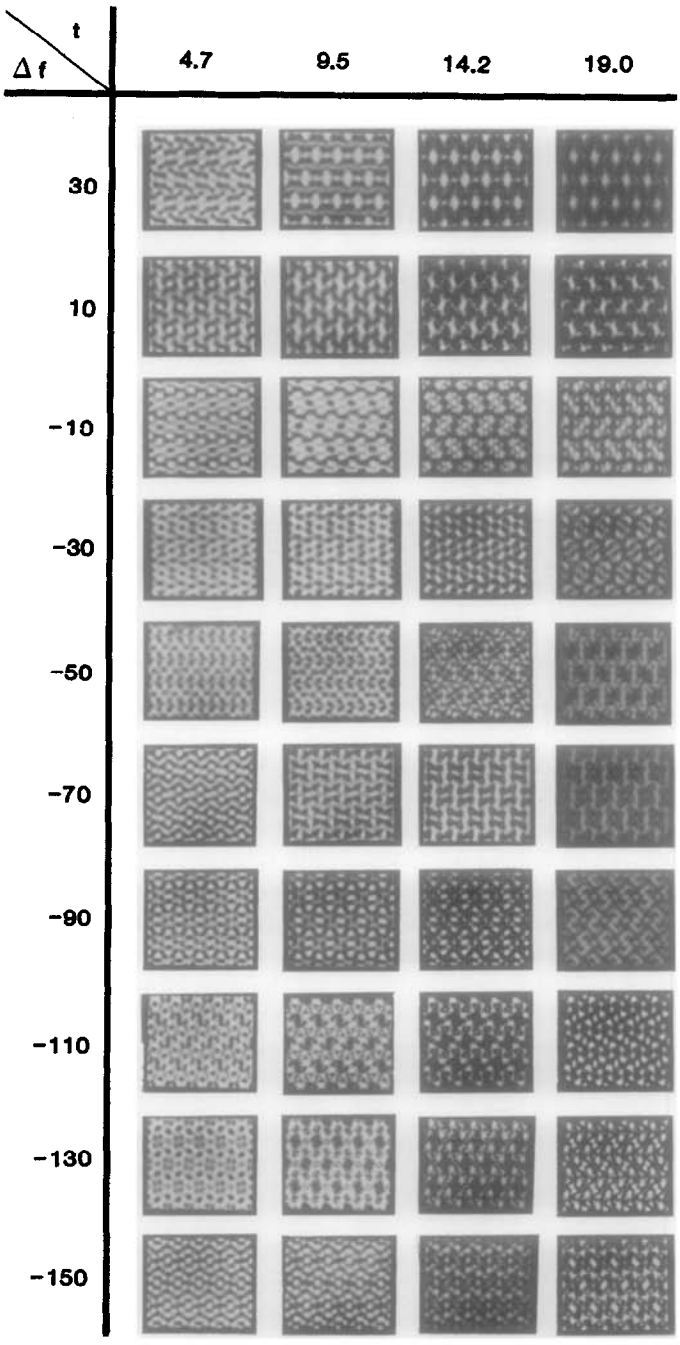

FIG. 12. Computer-simulated images of $Ce_4O_4S_3$ compounds of different thicknesses (t) and defocus values (Δf). Accelerating voltage = 200 kV, C_s = 1.2 mm, focus spread = 7 nm, and beam divergence = 8×10^{-4} rad.

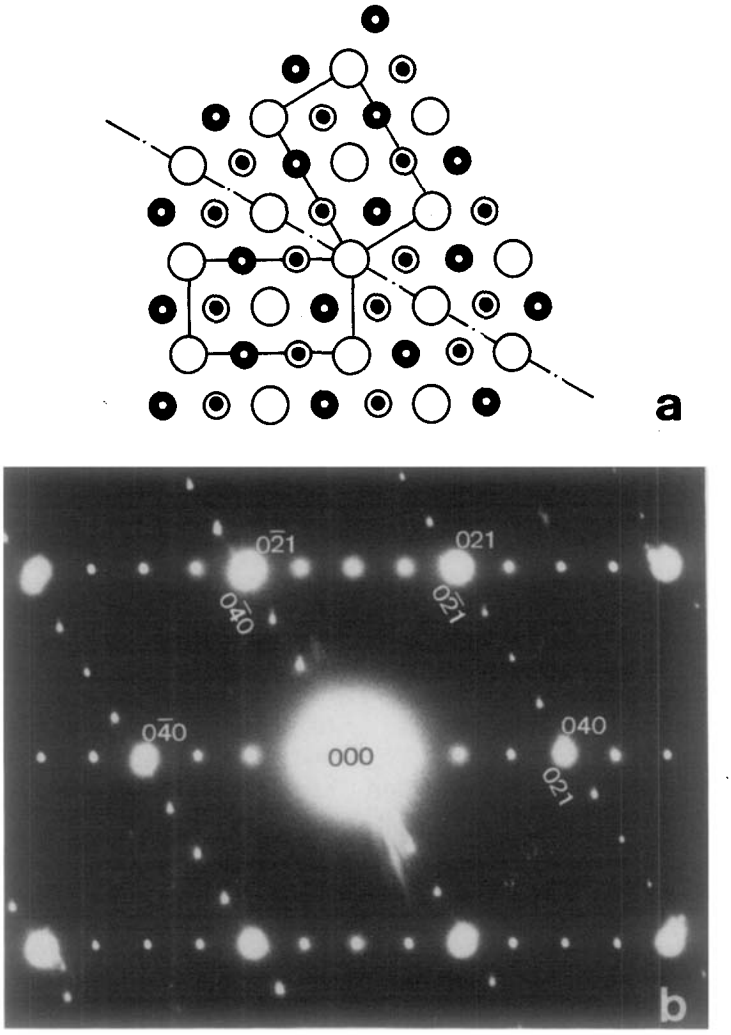

FIG. 13. Model (a) and diffraction pattern (b) of a twin in compound $n = 2$.

puted images. This is particularly the case for the relevant "bright bar contrast," which was used in imaging most of the quaternary compounds. For Δf in the range -50 to -70 nm (i.e., around Scherzer defocus), we obtained good fit with the observed image for the ternary compound (Fig. 11).

From the choice of the origin in the model we can conclude that the "bright bars" represent rows of sulfur columns. This is illustrated in Fig. 11 which compares the model, the simulated image (t = 19 nm, $\Delta f = -50$ nm for Fig. 11a; t = 14.2 nm, $\Delta f = -90$ nm for Fig. 11b), and the experimental image for $n = 2$ all at the same magnification.

From the interleaving of the sequences of "bright bars" in successive strips we conclude that the intuitive interpretation of the images in Figs. 7 and 8 in terms of block shifts is justified since the bright bars can in fact be considered images of the rows of sulfur columns.

6. Twinning

Diffraction patterns have also provided evidence for the occasional presence of twins in which the long parameter (i.e., the b axis) differs in orientation by 60° (or 120°). The two components of the twin belong to the same stacking variant $n = 2$. The row of "unsplit" spots in the diffraction pattern, i.e., the row through 021, which is perpendicular to the twin plane in real space, is clearly visible in Fig. 13b and leads to a (021) twin plane, when referred to the $n = 2$ lattice. The formation of twins of this type is not surprising since the layers of sulfur alone have very closely hexagonal symmetry. A model for this twin, as projected on the $(100)_o$ plane, is represented in Fig. 13a. The spot splitting along the row of spots normal to the unsplit row is consistent with the orthorhombic deformation of this hexagonal arrangement.

7. Discussion and Conclusions

Electron diffraction and high-resolution experiments have confirmed that the structures of the series of compounds $U_2La_{2n-2}O_{2n}S_{n+1}$ are stacking variants derived from the La_2O_2S structure by the introduction of periodic planar interfaces along which the excess sulfur is accommodated.

It was found that the interfaces are of a novel type. They separate domains in which the basic structures are rotated over an angle π about an axis normal to the interfaces; such a rotation is a symmetry operation for the sulfur sublattice but not for the arrangement of the other atoms. Moreover, the sulfur sublattices in the two domains are related by a parallel displacement which is of the type $\frac{1}{2}[100] + \varepsilon[010]$, where $\varepsilon[010]$ is a small displacement normal to the interfaces and results from the presence of excess sulfur atoms along the interfaces.

Although the X-ray diffraction experiments revealed only structures corresponding to integral values of n, i.e., of the $2\,\bar{2}$, $3\,\bar{3}$, type, electron microscopy allowed us to identify more complicated sequences such as $2\,\bar{3}$, $3\,\bar{4}$, $4\,\bar{5}$ and $4\,\bar{4}\,3\,\bar{4}\,4\,3$ corresponding to fractional values of n, respectively $\frac{5}{2}$, $\frac{7}{2}$, $\frac{9}{2}$, and $\frac{11}{3}$. The building principle in the corresponding crystal structures is the same as that of the compounds with n = integer.

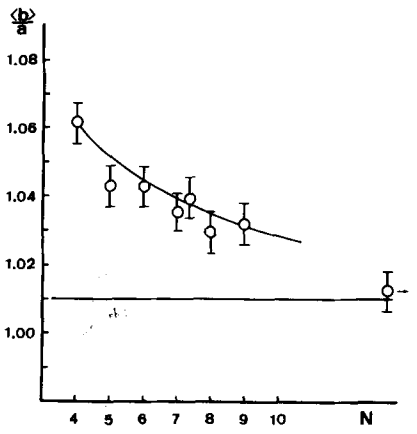

FIG. 14. Experimental $\langle b/a \rangle$ values for various members of the homologous series. From the curve fitting, a sulfur double-layer thickness of $\Delta = 0.036$ nm can be deduced.

The diffraction patterns of these materials exhibit features characteristic of the diffraction patterns of mixed layer compounds and can be analyzed on this basis. The new type of periodic interface produces characteristic extinctions in the diffraction pattern, which are similar to those associated with a twofold screw axis in ordered structures, but only for integral n values, because only then do the two slabs have the same thickness.

Appendix

Assuming that the structure blocks, as represented in Fig. 3, are the same size in all compounds we can write, for the superstructure, $b_s = nb + 2\Delta$, where b is the b parameter of the basic structure, i.e., corresponding to $N = \infty$, and Δ is the thickness of the double layer of sulfur atoms. The b

parameter derived from the diffraction pattern of compound $N = 2n$ is called the average b parameter, $\langle b \rangle = b_s/n$; we thus have the relationship

$$\langle b \rangle / a = (b/a)_\infty + (2\Delta/na)$$

which is represented in Fig. 14. The value of Δ can be deduced from $n(\langle b \rangle - b) = 2\Delta$. Within experimental error the observed values of $a/\langle b \rangle$ fit the curve for $\Delta = 0.036$ nm. The lattice parameters used were $a = 0.694$ nm, $b = 0.701$ nm, $c = 0.405$ nm, $(b/a)_\infty = 1.010$.

References

1. A. J. MORTON, *Phys. Status Solidi A* **31,** 661 (1975), **44,** 205 (1977); M. SNYKERS, R. SERNEELS, P. DELAVIGNETTE, R. GEVERS, AND S. AMELINCKX, *Crystal Lattice Defects* **3,** 99 (1972).
2. I. BAELE, G. VAN TENDELOO, AND S. AMELINCKX, *Acta Metall.* **35,** 401 (1987).
3. D. VAN DYCK, J. VAN LANDUYT, S. AMELINCKX, NGUYEN HUY-DUY, AND C. DRAGON, *J. Solid State Chem.* **19,** 179 (1976).
4. G. VAN TENDELOO, J. VAN LANDUYT, AND S. AMELINCKX, *Phys. Status Solidi A* **33,** 723 (1976).
5. G. VAN TENDELOO, D. VAN DYCK, S. KUYPERS, AND S. AMELINCKX, *Phys. Status Solidi A* **101,** 339 (1987).
6. VO VAN TIEN, M. GUITTARD, AND J. FLAHAUT, *J. Solid State Chem.*, in press.
7. J. DUGUE, D. CARRE, AND M. GUITTARD, *Acta Crystallogr. B* **34,** 3564 (1978).
8. J. DUGUE, D. CARRE, AND M. GUITTARD, *Acta Crystallogr. B* **35,** 1550 (1979).
9. B. MOROSIN AND D. J. NEWMAN, *Acta Crystallogr. B* **29,** 2647 (1973).
10. W. COENE AND D. VAN DYCK, *Ultramicroscopy* **15,** 41 (1984).